Predictive Control of Power Converters: Designs with Guaranteed Performance

Ricardo P. Aguilera, *Member, IEEE,* and Daniel E. Quevedo, *Senior Member, IEEE*

***Abstract*—In this work, a cost function design, based on Lyapunov stability concepts, for Finite Control Set Model Predictive Control is proposed. This predictive controller design allows one to characterize the performance of the controlled converter while providing sufficient conditions for local stability for a class of power converters. Simulation and experimental results on a buck dc-dc converter and a 2-level dc-ac inverter are conducted to validate the effectiveness of our proposal.**

***Index Terms*—Predictive control, power conversion, finite control set, controller performance, stability.**

I. Introduction

In the power electronics field, research has been focus on not only to obtain new advantageous converter topologies, but also to improve control methodologies to govern them [1], [2]. In this area, predictive control techniques have emerged as a promising control alternative for power converters [3]–[7]. Model Predictive Control (MPC) is a control strategy that obtains the control action by solving, at each sampling instant, an optimization which forecasts the future system behaviour over a finite horizon. The main advantage of MPC comes from the fact that system constraints (e.g., current and voltage limitations, and switch position) and non-linearities can be explicitly considered in the optimization [8].

Different predictive control approaches have been proposed to handle power converters, showing that these methods potentially have many advantages when compared to traditional PWM-based controllers. For recent applications of MPC for power converters see [9]–[13] while for electrical drives see [14]–[16]. Due to its flexibility and potentiality, Finite Control Set MPC (FCS-MPC) [4] is one of the most popular predictive controller for power converters. FCS-MPC directly considers the power switches in the optimization as constraints on the inputs [17]. Consequently, there is no need to use modulators.

Despite the good performance that FCS-MPC in principle offers, there remain several open problems, such as cost function design and the lack of stability guarantees. In the context of MPC, the infinite-horizon case, in general, ensures closed-loop stability provided that a solution with a finite cost exists [8]. Nevertheless, in power electronics, short horizons (commonly, horizon one solutions) are preferred due to practical limitations. For FCS-MPC, this problem becomes more involved due to the fact that this MPC strategy, in general, does not provide an explicit solution. This makes characterizing the resulting closed-loop performance a non-trivial task [17].

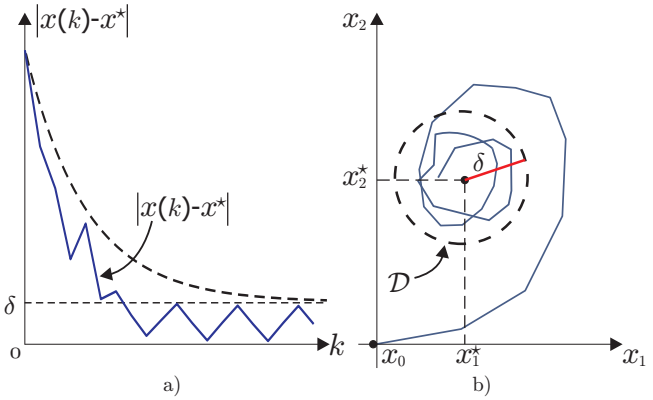

Fig. 1. Convergence of the converter state, $x(k)$, to the neighbourhood of the reference $x^\star$. a) Practical asymptotical stability; b) Ultimately bounded set $\mathcal{D}$: x will be confined in $\mathcal{D}$.

The above issues motivate one to focus on both deriving an explicit closed-loop solution and developing a cost function design method to guarantee closed-loop stability and performance of horizon-one FCS-MPC for power converters.

In the present work, a Lyapunov based stabilizing cost function design of horizon-one FCS-MPC for power converters is presented, which is an extension of the preliminar work presented in [18]. The key idea of this proposed approach is based on representing power converters as linear systems with quantized inputs. Additionally, a quadratic cost function, similar to the one used for convex MPC (or Explicit MPC), is considered [19]. Thus, FCS-MPC can be seen as a quantized version of convex MPC. Therefore, the advantage of using this proposed cost function comes from the fact that one can characterize the performance and stability of FCS-MPC in a similar fashion than in the convex MPC case, i.e., by using Lyapunov stability theory [20]. In this particular case, practical stability of the power converter state, $x(k)$, to a neighbourhood of the desired reference value $x^\star$ is established. In essence, as depicted in Fig. 1, it will be shown how to design the controller to ensure that the tracking error, $x(k) - x^\star$, decays in time until finally reaching a neighbourhood of the reference represented by $\mathcal{D}$. Thus, the decay rate of the tracking error and the radius of $\mathcal{D}$, δ, can be used to characterize the closed-loop performance of the power converter in terms of transient response and steady state error respectively. To validate the effectiveness of this proposal, simulations and experimental results on a buck dc-dc converter and a three-phase two-level

Manuscript received January 10, 2013. Accepted for publication October 2, 2014. The authors acknowledge the support of the Australian Research Council's Discovery Projects funding scheme (project number DP110103074).

R. P. Aguilera is with the Austrlian Energy Research Institue (AERI) at the School of Electrical Engineering and Telecommunication, The University of New South Wales, Sydney, Australia (e-mail: raguilera@ieee.org).

D. E. Quevedo is with the School of Electrical Engineering & Computer Science, The University of Newcastle, Australia (e-mail: dquevedo@ieee.org).

inverter governed by horizon-one FCS-MPC are carried out.

Notation: Let $\mathbb{R}$ and $\mathbb{R}_{\geq 0}$ denote the real and non-negative real numbers, respectively. The difference between two sets $\mathcal{A} \subseteq \mathbb{R}^n$ and $\mathcal{B} \subseteq \mathbb{R}^n$ is denoted by $\mathcal{A} \backslash \mathcal{B} \triangleq \{x \in \mathbb{R}^n : x \in \mathcal{A}, x \notin \mathcal{B}\}$. The transpose of a matrix A and a vector x are represented via $(Ax)^T = x^T A^T$. The maximum and minimum eigenvalues of a matrix A are $\lambda_{\max}(A)$ and $\lambda_{\min}(A)$, respectively. $|\cdot|$ represents the Euclidean norm. For any positive definite matrix P, $|x|_P^2 = x^T P x$ denotes the squared weighted Euclidean norm. A $n \times n$ identity matrix and a $n \times m$ zero matrix are denoted by $I_{n\times n}$ and $0_{n\times m}$ respectively.

II. Horizon-One Quadratic FCS-MPC

The focus of this work is on power converters that can be modeled, in a state space framework, via:

$$x(k+1) = Ax(k) + Bu(k), \tag{1}$$

where $x \in \mathbb{X} \subseteq \mathbb{R}^n$ stands for the n-system state variables (e.g. voltages and currents) and $u \in \mathbb{U} \subset R^m$ represents the m-control inputs of the power converter, i.e., the switch positions or voltage levels. Thus, this kind of input belongs to a finite control set of p elements, represented by

$$u(k) \in \mathbb{U} = \{u_1, u_2, \ldots, u_p\}. \tag{2}$$

The desired converter reference (e.g. output current) is represented by $x^\star \in \mathbb{R}^n$. Therefore, the control goal is represented by an equilibrium point via the target

$$x(k+1) = x(k) = x^\star. \tag{3}$$

Consequently, in this work, the idea is to govern this class of power converters via horizon-one FCS-MPC to achieve the desired reference $x^\star$. Standard examples of FCS-MPC for this class of systems can be found in [3]–[5].

A. Cost Function

In power electronics, system states represent variables of different physical nature and order of magnitude, e.g., currents, voltages, torques, power, etc. Thus, to evaluate the future behaviour of the power converter, it is convenient to adopt a cost function, which considers a weighted positive sum of the tracking errors of the controlled variables [5]. For example, for a two-level inverter, in $\alpha\beta$ coordinates, one can use

$$J_{2LI} = w_1(i_\alpha(k+1) - i^\star)^2 + w_2(i_\beta(k+1) - i^\star)^2, \tag{4}$$

where the weighting factors w_1 and w_2 are normally chosen as $w_1 = w_2 = 1$. In the case of a one-phase three-cell Flying Capacitor Converter (FCC), one can choose (see, e.g., [21])

$$\begin{aligned} J_{FCC} =& w_1(i_a(k+1) - i_a^\star)^2 + w_2(v_{c1}(k+1) - v_{c1}^\star)^2 \\ &+ w_3(v_{c2}(k+1) - v_{c2}^\star)^2, \end{aligned} \tag{5}$$

where normally $w_1 = 1$ and $w_2 = w_3$. Thus, the above cost functions can be expressed, in terms of the current state $x(k) = x$ and input $u(k) = u$, as

$$\begin{aligned} J(x,u) =& (x(k+1) - x^\star)^T P (x(k+1) - x^\star) \\ =& (Ax + Bu - x^\star)^T P (Ax + Bu - x^\star), \end{aligned} \tag{6}$$

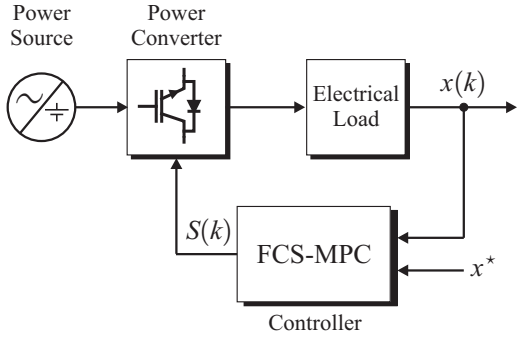

Fig. 2. MPC with finite control set.

where $P = \text{diag}\{w_1, \ldots, w_n\}$.

Inspired by the above, the focus of this work is on the following class of quadratic cost function (with $x(k) = x$):

$$V(x,u) = |x - x^\star|_Q^2 + |u - u^\star|_R^2 + |x(k+1) - x^\star|_P^2, \tag{7}$$

where matrices Q and R are semi-positive definite and P is positive definite. Additionally, $u^\star$ is the required input to keep (3) during the steady state. Thus, from (1) and (3), the steady state input, $u^\star$ can be obtained via

$$x^\star = (I - A)^{-1} B u^\star. \tag{8}$$

Clearly, (6) is a particular case of (7) where $Q = 0_{n\times n}$, $R = 0_{m\times m}$, and matrix P is given by the weighting factors w_i. Our subsequent analysis will reveal that by properly adjusting P the MPC loop can be designed to exhibit provable and desirable performance properties.

B. Optimal Control Input

Considering the current system state, $x(k) = x$, the optimal control input $u^{\text{opt}}(x)$ is obtained by minimizing the cost function $V(x,u)$ in (6) subject that the input belongs to the finite control set, $\mathbb{U}$ in (2). This optimization provides the optimal predictive control law, say:

$$u^{\text{opt}}(x) \triangleq \arg\{\min_{u\in\mathbb{U}} V(x,u)\}. \tag{9}$$

Consequently, the power converter presented in (1), governed by (9), yields the closed-loop equation

$$x(k+1) = Ax(k) + Bu^{\text{opt}}(x(k)). \tag{10}$$

This procedure is repeated at each sampling instant using fresh measurements of the system state. In Fig. 2, a block diagram of this predictive control strategy is presented.

III. Closed-Form Solution of Horizon-One FCS-MPC

In this section, the closed-form solution in the unconstrained case is recalled. Based on this nominal solution, the closed-form solution of horizon-one FCS-MPC is derived.

A. Unconstrained Optimum

Here, the ideal case where system constrains are not present is considered, i.e., $x \in \mathbb{R}^n$ and $u \in \mathbb{R}^m$. The cost function (7), with $\hat{x} = x - x^\star$ and $\hat{u} = u - u^\star$, can be re-written as

$$\begin{aligned} V(x,u) &= |\tilde{x}|_Q^2 + |\tilde{u}|_R^2 + |A\tilde{x} + B\tilde{u}|_P^2 \\ &= \tilde{x}^T(A^TPA + Q)\tilde{x} + \tilde{u}^T(B^TPB + R)\tilde{u} + 2\tilde{u}^TB^TPA\tilde{x}. \end{aligned} \tag{11}$$

In this case, the optimization in (9) results in the *unconstrained* optimal solution, $u_{uc}^{\text{opt}}(x)$, which can be obtained by making the partial derivative of the cost function equal to zero, i.e.,:

$$\frac{\partial V(\tilde{x},\tilde{u})}{\partial \tilde{u}} = 2(B^TPB + R)\tilde{u} + 2B^TPA\tilde{x} = 0. \tag{12}$$

Therefore, the minimizer to (7), *without taking into account any system constraints*, is given by

$$\begin{aligned} \tilde{u}_{uc}^{\text{opt}}(k) &= K\tilde{x}(k), \\ u_{uc}^{\text{opt}}(k) &= K(x(k) - x^\star) + u^\star, \end{aligned} \tag{13}$$

where

$$K = -W^{-1}B^TPA, \quad W = B^TPB + R. \tag{14}$$

It is worth noting that this nominal solution, $u_{uc}^{\text{opt}}(k)$, will generally *not belong to the finite set* $\mathbb{U}$ in (2).

B. Constrained Closed-Form Solution

In the case when MPC presents a finite control set constraint, the optimal solution, in general, is not necessarily the quantization of the unconstrained one. Based on [17], the expression of the optimal control input is given by

$$u^{\text{opt}}(k) = W^{-1/2}q_{\mathbb{V}}\left(W^{1/2}u_{uc}^{\text{opt}}(k)\right), \tag{15}$$

where $u^{\text{opt}}(k)$ belongs to the finite set $\mathbb{U}$. For the sake of brevity, the analysis to obtain (15) has been neglected. Nevertheless, for further details the interested reader is referred to [17], [22].

In essences, (15) tells one that to obtain the constrained optimum, u^{opt}, one must first perform a linear transformation of the finite control inputs, $\mathbb{U}$, using $W^{1/2}$, i.e., $\mathbb{V} = W^{1/2}\mathbb{U}$. Thus, in this new space, one can perform the quantization $q_{\mathbb{V}}(\cdot)$. The term $W^{-1/2}$ represents, then, the inverse transform. A block diagram of the resulting one-step FCS-MPC closed-loop is depicted in Fig. 3.

Now, the optimal constrained solution can be re-written as:

$$u^{\text{opt}}(k) = u_{uc}^{\text{opt}}(x) + W^{-1/2}\eta_{\mathbb{V}}(x), \tag{16}$$

where $\eta_{\mathbb{V}}$ stands for the quantization error. Consequently, the closed-loop recursions becomes

$$x(k+1) = A_K(x(k) - x^\star) + x^\star + BW^{-1/2}\eta_{\mathbb{V}}(x) \tag{17}$$

where $A_K \triangleq A + BK$.

It is important to emphasize that obtaining the optimal input, $u^{\text{opt}}(k)$, by solving the minimization as per (9) is equivalent to performing the quantization of the unconstrained solution as per (15). Thus, closed-loop systems (10) and (17) are equivalent. This opens the door to develop fast algoritms to obtain the optimal control law, $u^{\text{opt}}(x)$, see [22]–[24]

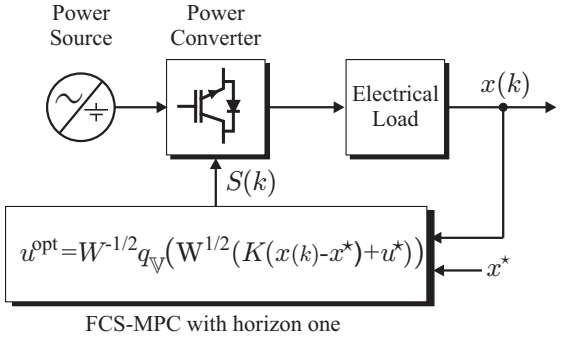

Fig. 3. Horizon-one FCS-MPC closed-loop.

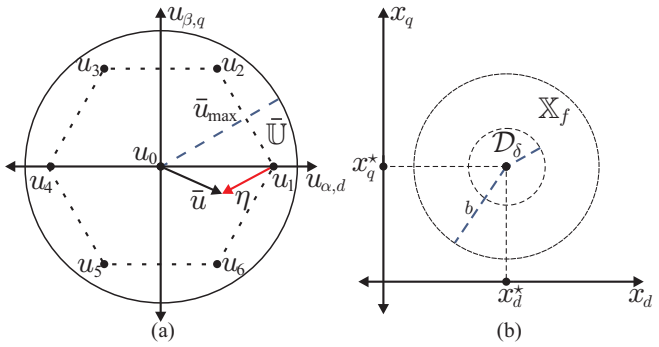

Fig. 4. Sets involved in the cost function design; (a) Finite control set $\mathbb{U}$ and nominal input set $\bar{\mathbb{U}}$; (b) Terminal region $\mathbb{X}_f$ and bounded set $\mathcal{D}_\delta$.

IV. Cost Function Design for Performance

Here, ideas used for convex MPC formulations, such as Explicit MPC [19] are adapted to design matrix P to guarantee stability (as in Fig. 1) and derive performance bounds of FCS-MPC. Given the nature of this problem, and in view of results for unconstrained systems (see Chapter 2.5 in [8]), this work proposes to design the quadratic cost function (7) by choosing matrix P as the solution of the algebraic Riccati equation

$$A_K^TPA_K - P + Q + K^TRK = 0, \tag{18}$$

where K is as in (14). This guarantees that A_K is Schur stable, i.e., $|\lambda_i(A_K)| < 1$ for all $i \in \{1, \ldots, n\}$ [25].

A. Preliminaries

To obtain a bound for the quantization error, firstly, the following *nominal input set* for the finite control set $\mathbb{U}$, in (2), is introduced

$$\bar{\mathbb{U}} \triangleq \{\bar{u} \in \mathbb{R}^m : |\bar{u}| \leq \bar{u}_{\max}\}, \tag{19}$$

where $\bar{u}_{\max} \in (0, \infty)$ is a design parameter. Since $\bar{\mathbb{U}}$ is bounded, so is the quantization error in $\mathbb{U}$, thus

$$|\eta_{\mathbb{U}}| \leq \Delta_q \triangleq \max_{\bar{u} \in \bar{\mathbb{U}}} |q_{\mathbb{U}}(\bar{u}) - \bar{u}| < \infty. \tag{20}$$

Note that Δ_q depends upon $\bar{u}_{\max}$. To clarify the concept of *nominal input set*, the following example is given:

Example 1 (Two-Level Inverter): In Fig. 4. the typical vectorial representation of a 2-level inverter output voltages in the $\alpha\beta$ (or dq) coordinates is presented. The finite input set,

$\mathbb{U}$, contains the 7 inverter vectors, which are contained by the nominal input set, $\bar{\mathbb{U}}$, i.e.,

$$\mathbb{U} = \{u_0, \dots, u_6\} \subset \bar{\mathbb{U}} \subset \mathbb{R}^2. \tag{21}$$

In this case, the quantization of the nominal input $\bar{u} \in \bar{\mathbb{U}}$ is given by $q_{\mathbb{U}}(\bar{u}) = u_1$, thus $\eta_{\mathbb{U}}(\bar{u}) = u_1 - \bar{u}$. Notice that for the dq framework, the inverter vectors will be rotating. However, they always will be contained by the nominal input set, $\bar{\mathbb{U}}$, producing the same maximum quantization error Δ_q as in the $\alpha\beta$ framework. ∎

From the unconstrained solution in (13), the following nominal local controller is introduced:

$$u_f(x) = u_{uc}^{\text{opt}}(x) = K(x - x^\star) + u^\star. \tag{22}$$

This motivates us to define a *terminal region* as

$$\mathbb{X}_f \triangleq \left\{ x \in \mathbb{R}^n : |x - x^\star| \leq b = \frac{\bar{u}_{\max} - |u^\star|}{|K|} \right\} \tag{23}$$

Thus, this terminal region guarantees, from (20), that the quantization error will be bounded, i.e.:

$$|\eta_{\mathbb{U}}(u_f(x))| \leq \Delta_q, \quad \forall x \in \mathbb{X}_f. \tag{24}$$

It is important to emphasize that each system state, x, which belongs to the proposed terminal region, $\mathbb{X}_f$, produces a nominal input, $u_f(x)$, which belongs to the nominal input set $\bar{\mathbb{U}}$, i.e., $\kappa_f(x) \in \bar{\mathbb{U}}$ for all $x \in \mathbb{X}_f$.

B. Performance Guarantees

By extending [26], next, it will be shown how to design the MPC cost function to guarantee stability and performance.

Theorem 1: Consider the following positive constants: $a_1 = \lambda_{\min}(P)$, $a_2 = \lambda_{\max}(P)$, $a_3 = \lambda_{\min}(Q)$, $a_4 = |W|$, and $\rho = 1 - \frac{a_3}{a_2}$. Let

$$\mathcal{D}_\delta \triangleq \{x \in \mathbb{R}^n : |x - x^\star| \leq \delta\} \tag{25}$$

$$\delta^2 = \frac{a_4}{a_1(1-\rho)} \Delta_q^2 \tag{26}$$

be a neighbourhood of the reference $x^\star$. Suppose that matrix P is chosen as per (18). If Δ_q in (20) is bounded by

$$\Delta_q^2 \leq \left(\frac{a_1 - a_2\rho}{a_4} \right) b^2, \tag{27}$$

then, the power converter (1) governed by horizon-one FCS-MPC (9) or (15) will be led to the neighbourhood $\mathcal{D}_\delta$, i.e.,

$$\limsup_{k \to \infty} |x(k) - x^\star| \leq \delta \tag{28}$$

for all $x(0) \in X_{MPC}$, where

$$X_{MPC} \triangleq \mathbb{X}_f \cup \{x \in \mathbb{R}^n : g(x) < 0\}. \tag{29}$$

$$g(x) = -a_3(x(k) - x^\star)^T(x(k) - x^\star) + a_4|\nu_{\mathbb{U}}(x)|^2 \tag{30}$$

The proof of this theorem can be found in Appendix A. ∎

Theorem 1 tells one that if the cost function is designed as per (18), and the quantization error is bounded by (27), then any initial state $x(0) \in X_{MPC}$ will be steered by the predictive control law, $u^{\text{opt}}(x)$, towards the terminal region $\mathbb{X}_f$ and then to the ultimately bounded set, $\mathcal{D}_\delta$, where the system will be eventually confined (see Fig. 1).

Algorithm 1 Region of Attraction $X_{MPC} \subseteq \mathbb{R}^2$

function X_{MPC} = XMPC($\mathbb{U}$, K, $u^\star$, a_3, a_4, $j_{\max}$)
  Initialization: $r \leftarrow b$, $\Delta r \leftarrow 0.01$, $j \leftarrow 1$
  while $j < j_{\max}$ **do**
    $\mathbb{X}_{MPC} \leftarrow \mathcal{B}_r$
    $r \leftarrow b + \Delta r$
    for $k = 1 : 360$ **do**
      $\tilde{x}(1,1) \leftarrow r\cos(2\pi(k-1)/360)$
      $\tilde{x}(2,1) \leftarrow r\sin(2\pi(k-1)/360)$
      $u \leftarrow K\tilde{x} - u^\star$ ▷ **See** (13)
      $d_{\min}^2 \leftarrow \infty$
      for $l = 1 : p$ **do**
        $d^2 \leftarrow (u - \mathbb{U}(:,l))^T(u - \mathbb{U}(:,l))$
        if $d^2 \leq d_{\min}^2$ **then**
          $d_{\min}^2 \leftarrow d^2$
        end if
      end for
      $g(x) \leftarrow -a_3\tilde{x}^T\tilde{x} + a_4 d_{\min}^2$ ▷ **See** (30)
      if $g(x) \geq 0$ **then**
        $j \leftarrow j_{\max}$
      end if
    end for
    $j \leftarrow j + 1$
  end while
end function

To determine the region of attraction of the proposed controller, X_{MPC} in (29), one can enlarge $\mathbb{X}_f$ by guaranteeing that $g(x) \leq 0$. However, outside $\mathbb{X}_f$, the quantization error, $\eta_U(x)$, will be larger than Δ_q. Thus, X_{MPC} can be obtained numerically, by using Algorithm 1. Since the closed loop (10) may be globally stable, i.e., $X_{MPC} = \mathbb{R}^n$, $j_{\max}$ is used to stop the algorithm. If the resulting ball is larger than the state constraints, then $X_{MPC} = \mathbb{X}$.

C. FCS-MPC Design Procedure

The proposed FCS-MPC design can be summarized in the following procedure.

1) Set the desired control goal, i.e., system reference, $x^\star$, and the steady state input, $u^\star$, which satisfies (8).
2) Set the cost function weighting matrices Q and R. It is convenient to define the system model in per-unit. Thus, every system tracking error, $x_i(k) - x_i^\star$, will be comparable. Therefore, one can choose $Q = I_{n\times n}$, and then only adjust R.
3) Calculate matrix P from (18). This can be easily done in Matlab by using the command *dlqr*.
4) Calculate K and W from (14).
5) Choose the nominal control set $\bar{\mathbb{U}}$, by setting $\bar{u}_{\max}$. This determines the maximum quantization error Δ_q.
6) Check the stability condition (27). If (27) is not satisfied, modify matrix R and repeat steps 3)–6).
7) With K and $\bar{u}_{\max}$, obtain the terminal region $\mathbb{X}_f$ in (23).
8) Calculate ρ and $\mathcal{D}_\delta$. Here, the decay rate ρ determines the speed that the system state x is led to the reference,

$x^\star$, in the terminal region $\mathbb{X}_f$ while δ determines the maximum steady state error.

9) To obtain the region of attraction of the horizon-one FCS-MPC, X_{MPC}, enlarge $\mathbb{X}_f$ by using Algorithm 1.

Notice that, by modifying matrix R, one can adjust the transient respond and steady state error of the proposed predictive controller. With a larger matrix R, one seeks to apply an input close to $u^\star$. This allows one to reduce the control action that is applied to the system, leading to a slower dynamic response (less aggressive controller) with often better robustness properties. Nevertheless, since $u^\star$ may not be part of the finite control set, the optimization for large matrix R tends to become the quantization of the steady-state input, i.e., $u^{\text{opt}} \approx q\{u^\star\}$. Thus, FCS-MPC may decide to keep the power switch always open or closed. Since power converters are in general open-loop stable systems, i.e., $|\lambda_{\max}(A)| < 1$, the system state will not diverge. However, the closed-loop system will exhibit the largest possible steady-state error, i.e., the largest region $\mathcal{D}$. Thus, decreasing matrix R will stimulate power switches commutation, reducing the size of $\mathcal{D}$ while increasing commutation losses. Consequently, if condition (27) is not satisfied, the system will not diverge infinitely. Nevertheless, it is not possible to characterize its performance.

V. Simulation Study: Buck DC-DC Converter

This power converter, presented in Fig. 5, contains three power switches. Each of them can adopt only two values, i.e., $S_i = 0$ if the switch is open and $S_i = 1$ when it is closed. Thus, $S_i \in \{0, 1\}$, for all $i \in \{1, 2, 3\}$. It is clear that, to avoid internal faults, some of the switch combinations are forbidden. If the switching input vector is defined as: $s(t) = \begin{bmatrix} S_1(t)^T & S_2(t)^T & S_3(t)^T \end{bmatrix}^T$, then it will be restricted to belong to the following finite control set:

$$s(t) \in \left\{ \begin{bmatrix} 0 \\ 0 \\ 1 \end{bmatrix}, \begin{bmatrix} 0 \\ 1 \\ 0 \end{bmatrix}, \begin{bmatrix} 1 \\ 0 \\ 0 \end{bmatrix} \right\}. \tag{31}$$

This is equivalent to considering the input voltage, $v_i(t)$, as control input, which is constrained according to:

$$v_i(t) \in \mathbb{V} \triangleq \left\{ 0, \frac{V_{dc}}{2}, V_{dc} \right\}. \tag{32}$$

Considering a base voltage, $V_{base} = V_{dc}$, and a base current, $I_{base} = V_{dc}/r$, the discrete-time per unit model of the buck DC-DC converter is expressed by:

$$\begin{aligned} i_{L,pu}(k+1) &= i_{L,pu}(k) - \frac{hr}{L} v_{o,pu}(k) + \frac{hr}{L} v_{i,pu}(k), \\ v_{o,pu}(k+1) &= \frac{h}{rC} i_{L,pu}(k) + \left(1 - \frac{h}{rC}\right) v_{o,pu}(k), \end{aligned} \tag{33}$$

where h is the sampling period. Here, $x = \begin{bmatrix} i_{L,pu} & v_{o,pu} \end{bmatrix}^T$ is the system state, while the control input is $u = v_{i,pu}$.

The output voltage reference can be defined as $v_o^\star = \alpha V_{dc}$, with $\alpha \in (0, 1)$. From the system model, one can see that this voltage reference will be reached when the inductor current is $i_L^\star = v_o^\star / r = \alpha V_{dc}/r$. On the other hand, the required voltage input, $v_i^\star$, to keep this desired steady state is $v_i^\star = v_o^\star = \alpha V_{dc}$. Thus, the per-unit references become $i_{L,pu}^\star = v_{o,pu}^\star = \alpha$.

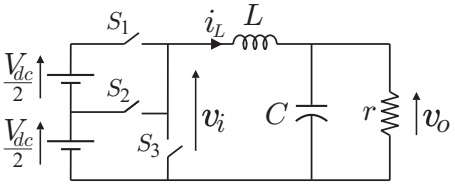

Fig. 5. Three-level buck dc-dc converter.

Notice that the output voltage reference, $v_o^\star = \alpha V_{dc}$, may not be an element of the finite set $\mathbb{V}$ in (32). Therefore, it is not always possible to achieve an equilibrium point. Thus, the best one can hope for, is that state trajectories be bounded near the desired reference. It is for this reason the focus of this work is on practical stability as studied in Section IV.

Considering $\tilde{x} = \begin{bmatrix} i_{L,pu} - \alpha & v_{o,pu} - \alpha \end{bmatrix}^T$ and $\tilde{u} = v_{i,pu} - \alpha$, the buck dc-dc converter per-unit model is expressed via:

$$\tilde{x}(k+1) = A\tilde{x}(k) + B\tilde{u}(k), \tag{34}$$

$$A = \begin{bmatrix} 1 & -\frac{hr}{L} \\ \frac{h}{rC} & 1 - \frac{h}{rC} \end{bmatrix}, \quad B = \begin{bmatrix} \frac{hr}{L} \\ 0 \end{bmatrix}. \tag{35}$$

Thus, since $v_i \in \mathbb{V}$, the control input, $\tilde{u}$, is restricted to belong to the finite set $\tilde{\mathbb{U}}$ expressed via:

$$\tilde{u}(k) \in \tilde{\mathbb{U}} \triangleq \left\{ -\alpha, \quad \tfrac{1}{2} - \alpha, \quad 1 - \alpha \right\}. \tag{36}$$

Consider that, for safety reasons, it is required to operate the converter under the following conditions: $0 < i_{L,pu} < i_{\max}$ and $0 < v_{o,pu} < v_{\max}$. Hence, the system state, x, is restricted to belong to the set $\mathbb{X}$ defined by:

$$\mathbb{X} = \left\{ x \in \mathbb{R}^2 : x_1 \in [0, \ i_{\max}], x_2 \in [0, \ v_{\max}] \right\} \tag{37}$$

Consequently, the control objective is to steer any system state, $x \in \mathbb{X}$, to the origin.

For this simulation study, the electrical parameters of this DC-DC converter, depicted in Fig. 5, are chosen as $V_{dc} = 100V$, $r = 5\Omega$, $L = 3mH$ and $C = 110\mu F$. The desired output voltage reference is set as $v_o^\star = 37.5V$; thus, $\alpha = 0.375$. Thus, in this case, the finite control set is

$$\tilde{\mathbb{U}} = \left\{ -0.375, \quad 0.125, \quad 0.625 \right\}. \tag{38}$$

The predictive controller was implemented using a sampling period of $h = 200\mu s$. To design the cost function, the value of the weighting matrix Q is chosen in a similar manner for standard FCS-MPC (see P in (6)). Since the system is in per unit, both tracking errors have the same importance. On the other hand, matrix R will be chosen as design parameter to adjust the terminal region $\mathbb{X}_f$ and the ultimately bounded set $\mathcal{D}_\delta$. Thus, in this case, Q are R are chosen as

$$Q = I_{2\times 2}, \quad R = 0.25. \tag{39}$$

Then, matrix P is designed by solving the Riccati equation presented in (18). This can be easily obtained using MATLAB. Thus, for this case, it results in:

$$P = \begin{bmatrix} 2.4393 & 0.0589 \\ 0.0589 & 1.8784 \end{bmatrix}, \quad K = \begin{bmatrix} -1.5743 & 0.4962 \end{bmatrix}. \tag{40}$$

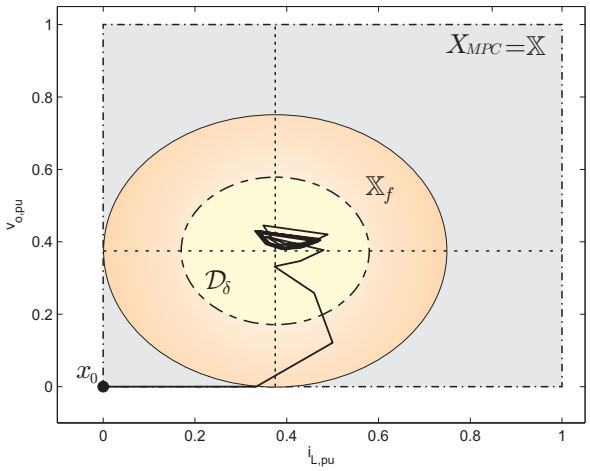

Fig. 6. Convergence of the buck converter to the bounded set $\mathcal{D}_\delta$; $R = 0.25$.

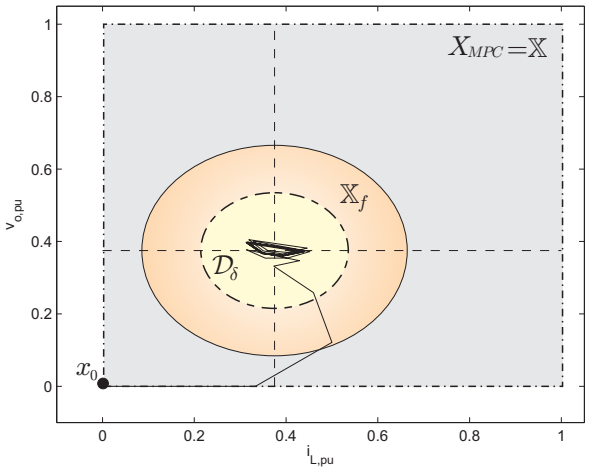

Fig. 9. Convergence of the buck converter to the bounded set $\mathcal{D}_\delta$; $R = 0.1$.

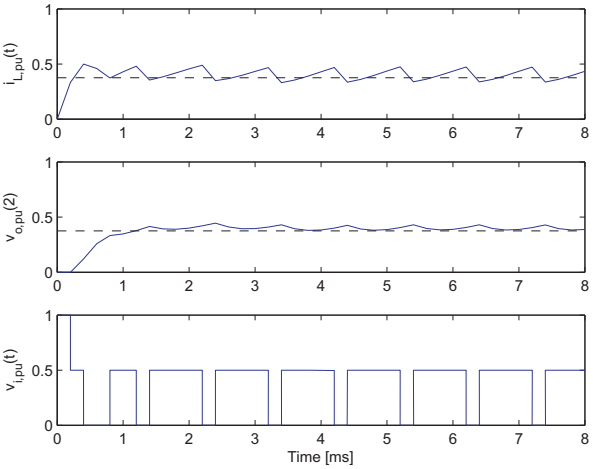

Fig. 7. System state and input trajectories.

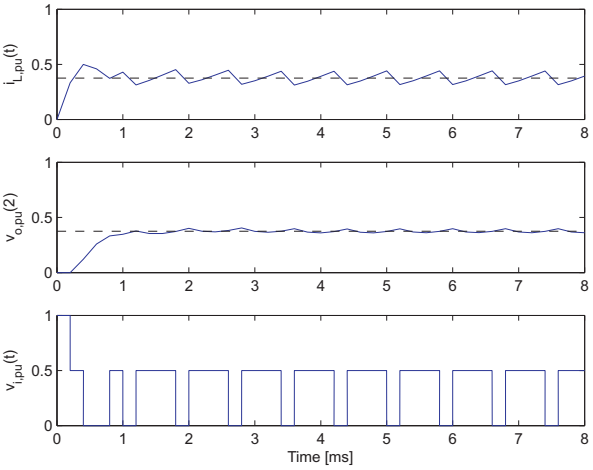

Fig. 10. System state and input trajectories.

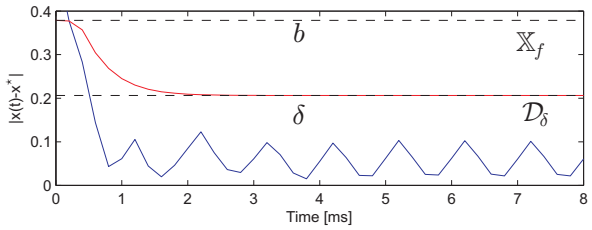

Fig. 8. Norm of the state deviations $|x(k) - x^\star|$.

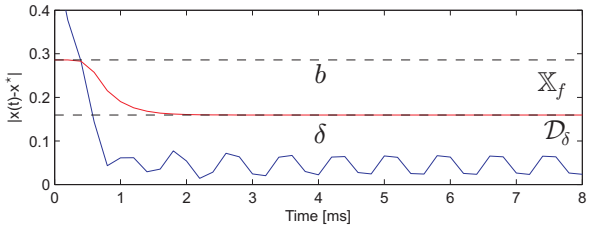

Fig. 11. Norm of the state deviations $|x(k) - x^\star|$.

Based on the finite control set $\tilde{\mathbb{U}}$, the following nominal control set is considered:

$$\bar{\mathbb{U}} \triangleq \{\bar{u} \in \mathbb{R}^m : |\bar{u}| \leq \bar{u}_{\max} = 0.625\}, \tag{41}$$

which provides, from (20), that

$$|\eta_{\mathbb{U}}| \leq \Delta_q = 0.25, \tag{42}$$

for all $\bar{u} \in \bar{\mathbb{U}}$. The terminal region can be characterized via:

$$\mathbb{X}_f \triangleq \left\{x \in \mathbb{R}^n : |x - \alpha| \leq b = \frac{\bar{u}_{\max}}{|K|} = 0.3787\right\}, \tag{43}$$

where $\tilde{u}^\star = 0$. Now, it is possible to verify that condition (27) in Theorem 1 is satisfied by:

$$\Delta_q^2 = 0.0625 < \left(\frac{a_1 - a_2\rho}{a_4}\right) b^2 = 0.2107, \tag{44}$$

The terminal region $\mathbb{X}_f$, thus, is an invariant set. Therefore, one can anticipate that the system state, x, will be led by the predictive controller to the ultimately invariant set:

$$\mathcal{D}_\delta \triangleq \{x \in \mathbb{R}^n : |x - \alpha| \leq \delta = 0.2062\}. \tag{45}$$

Clearly, $\mathcal{D}_\delta$ is contained in $\mathbb{X}_f$, i.e., $\mathcal{D}_\delta \subset \mathbb{X}_f$. Then, by invoking Algorithm 1, it is possible to find that $X_{MPC} = \mathbb{X}$.

The evolution of the buck converter under the proposed horizon-one FCS-MPC, starting from $v_{o,pu} = i_{L,pu} = 0$, is depicted in Fig. 6. Here, one can see that the predictive

controller leads the system state to the bounded set $\mathcal{D}_\delta$. The per-unit system state (inductor current $i_{L,pu}$ and output voltage $v_{o,pu}$) and the finite control input (input voltage $v_{i,pu}$) trajectories are shown in Fig. 7. It is clear that the steady-state system trajectories are bounded around the reference.

Due to the design of the cost function, $V(x)$, one can see in Fig. 8 that $|x(k) - x^\star|$ is exponentially bounded as shown in (85). Hence, when $x(k) \in \mathbb{X}_f$, it decreases exponentially, with a decay factor of $\rho = 0.5888$, until the system tracking error, $x(k) - x^\star$, reaches the bounded set $\mathcal{D}_\delta$. Inside this region, the tracking error, $x(k) - x^\star$, presents an oscillating behaviour bounded by δ. This is attributable to the fact that due to the switching action, which occurs at discrete time-instants, the system cannot reach an equilibrium point for such reference.

To show how the cost function design affects the system behaviour, a new simulation for the buck converter using a different matrix R, namely, $R = 0.1$, is carried out.

Following the same procedure used previously, it is obtained that

$$P = \begin{bmatrix} 1.8898 & 0.2307 \\ 0.23071 & 1.7284 \end{bmatrix}, \quad K = [\ -2.1224\ 0.5196\ ] \quad (46)$$

Now, the terminal region can be characterized via:

$$\mathbb{X}_f \triangleq \left\{ x \in \mathbb{R}^n : |x - \alpha| \leq b = \frac{\bar{u}_{\max}}{|K|} = 0.286 \right\}, \quad (47)$$

while the ultimately bounded set is expressed by:

$$\mathcal{D}_\delta \triangleq \{ x \in \mathbb{R}^n : |x - \alpha| \leq \delta = 0.1595 \}. \quad (48)$$

The results for this new cost function setting are presented in Figs. 9–11. When comparing both situations, it is clear that reducing the value of R, reduces the average steady-state error, which is normally observed in this kind of predictive control strategy, see [12]. However, it is achieved by increasing the number of commutations.

VI. Experimental Results: Two-Level Inverter

In this section, the stability and performance analysis presented in this work when applied to a three-phase two-level inverter is experimentally verified.

A. Two-Level Inverter Model

The topology of this inverter is presented in Fig. 12. The continuous-time dynamic model for each output current, i_y, is

$$\frac{di_y(t)}{dt} = -\frac{r}{L} i_y(t) + \frac{1}{L}(V_{dc} s_y(t) - v_{no}(t)), \quad \forall y \in \{a, b, c\}, \quad (49)$$

where v_{no} stands for the common mode voltage defined as $v_{no}(t) = \frac{1}{3}(v_{ia}(t) + v_{ib}(t) + v_{ic}(t))$. The input, s_y, belongs to the following finite set

$$\mathbb{S} \triangleq \left\{ \begin{bmatrix} 0 \\ 0 \\ 0 \end{bmatrix}, \begin{bmatrix} 0 \\ 0 \\ 1 \end{bmatrix}, \begin{bmatrix} 0 \\ 1 \\ 0 \end{bmatrix}, \begin{bmatrix} 0 \\ 1 \\ 1 \end{bmatrix}, \begin{bmatrix} 1 \\ 0 \\ 0 \end{bmatrix}, \begin{bmatrix} 1 \\ 0 \\ 1 \end{bmatrix}, \begin{bmatrix} 1 \\ 1 \\ 0 \end{bmatrix}, \begin{bmatrix} 1 \\ 1 \\ 1 \end{bmatrix} \right\}. \quad (50)$$

It is well known that, for sinusoidal references in a 3-phase system, one can apply the so-called abc-to-dq transformation. Firstly, the current vector in abc frame is defined as: $i_{abc} = [i_a\ i_b\ i_c]^T$. Then, it is transformed into dq frame by applying the following transformation:

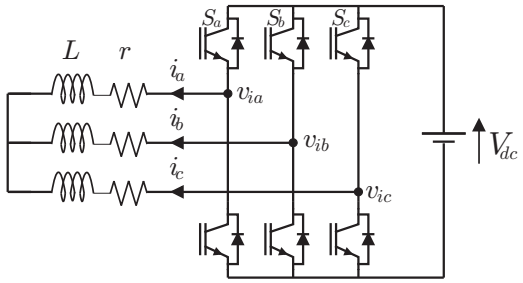

Fig. 12. Two-Level inverter topology.

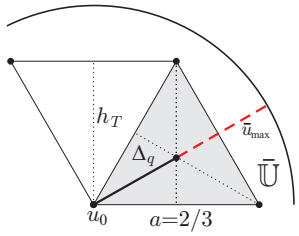

Fig. 13. Associated nominal control set $\bar{\mathbb{U}}$ for the 2-level inverter.

$$i_{dq}(t) = \Gamma(t) i_{abc}(t), \quad (51)$$

where:

$$\Gamma(t) = \frac{2}{3} \begin{bmatrix} \sin(\omega t) & \sin(\omega t - \frac{2\pi}{3}) & \sin(\omega t + \frac{2\pi}{3}) \\ \cos(\omega t) & \cos(\omega t - \frac{2\pi}{3}) & \cos(\omega t + \frac{2\pi}{3}) \end{bmatrix}, \quad (52)$$

and $i_{dq}(t) = [i_d(t) \quad i_q(t)]^T$.

Thus, considering $x = i_{dq}$ and $u = s_{dq}$, the discrete-time model of the 2-level inverter, in dq frame, is expressed by:

$$x(k+1) = Ax(k) + Bu(k), \quad (53)$$

$$A = \begin{bmatrix} 1 - h\frac{r}{L} & \omega h \\ -\omega h & 1 - h\frac{r}{L} \end{bmatrix}, \quad B = \begin{bmatrix} \frac{h}{L} V_{dc} & 0 \\ 0 & \frac{h}{L} V_{dc} \end{bmatrix}, \quad (54)$$

in which

$$u(k) \in \mathbb{U}(k) = \Gamma(k)\mathbb{S}. \quad (55)$$

In this case, constant amplitud reference, $I^\star$, is desired for the output currents i_{abc}. This is equivalent to setting

$$x^\star = i^\star_{dq} = [I^\star\ 0]^T. \quad (56)$$

The input required to keep this state value is given by

$$u^\star = s^\star_{dq} = [rI^\star / V_{dc} \quad \omega L I^\star / V_{dc}]^T. \quad (57)$$

B. Experimental Results

Here, experimental results of the performance of FCS-MPC when applied to a three-phase two-level inverter are presented. The inverter prototype was built based on discrete insulated-gate bipolar transistors (IGBTs) IRG4PC30KD. The electrical parameters of the converter-load system are $V_{dc} = 200\ V$, $r = 5\ \Omega$ and $L = 17\ mH$, see Fig. 12. The predictive strategy was implemented in a standard TMS320C6713 DSP considering a sampling period of $h = 100\ \mu s$. Then, the optimal input was

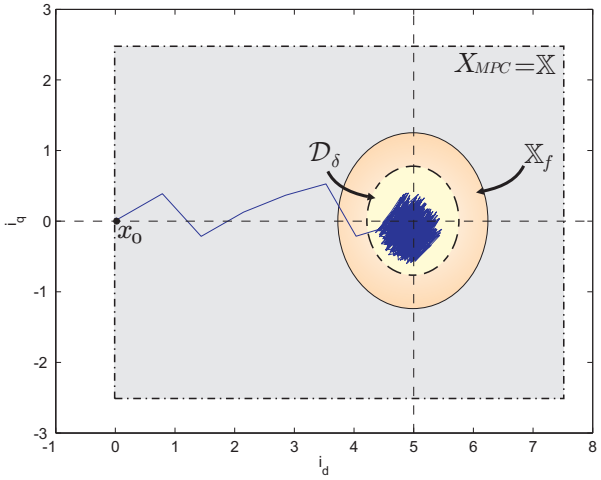

Fig. 14. Convergence of the 2-level inverter: $R = 2I_{2\times 2}$.

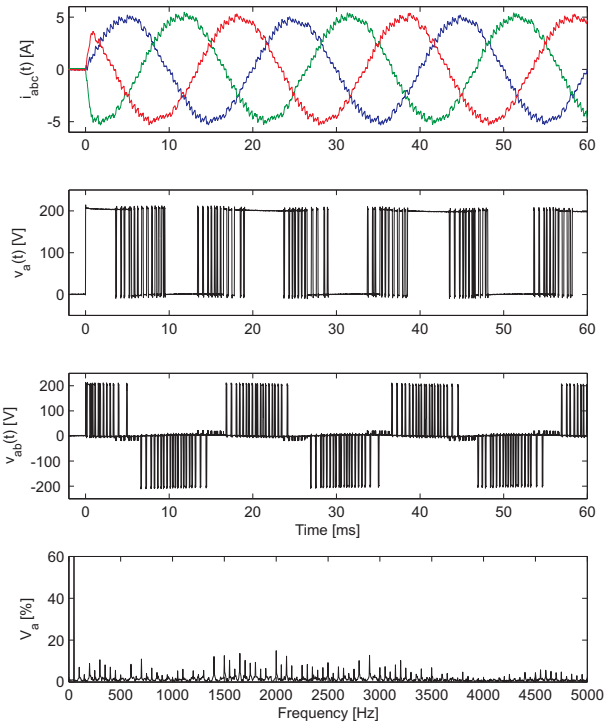

Fig. 15. System state and input trajectories, and inverter voltage spectrum.

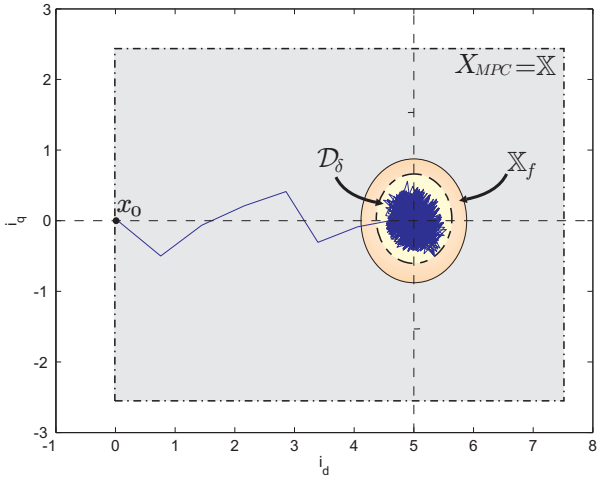

Fig. 16. Convergence of the 2-level inverter: $R = 0.0001I_{2\times 2}$.

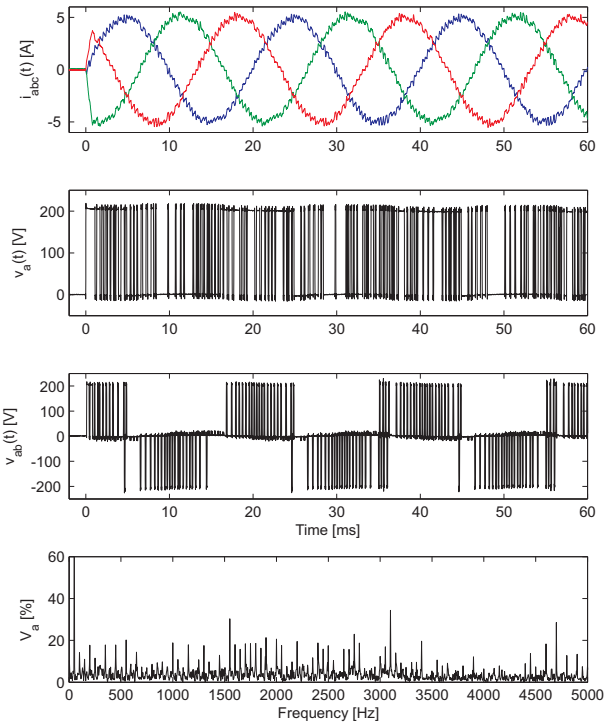

Fig. 17. System state and input trajectories, and inverter voltage spectrum.

applied to the converter by using an XC3S400 FPGA. The desired amplitude for the output current is $I^\star = 5\ A$ with a frequency of $f_0 = 50\ Hz$.

In this case, the cost function was set with $Q = I_{2x2}$ and $R = 2I_{2x2}$. Thus, following the proposed stabilizing design, one obtains that

$$P = 1.7455 I_{2\times 2}, \quad K = \begin{bmatrix} -0.4514 & -0.0146 \\ 0.0146 & -0.4514 \end{bmatrix}. \tag{58}$$

A key observation is that the time-varying finite control set, $\mathbb{U} = \Gamma(k)\mathbb{S}$, can be bounded by a fixed nominal set $\bar{\mathbb{U}}$. In Fig. 13, one can see that when the nominal input $\bar{u}$ is inside the hexagon boundary, the maximum quantization error, Δ_q, is given by the centroid or geometric center of the equilateral triangle formed by the adjacent inverter vectors. Thus, considering that $a = 2/3$, it follows that

$$h_T = \frac{\sqrt{3}}{2} a = \frac{\sqrt{3}}{3}. \tag{59}$$

Therefore, the maximum quantization error is given by:

$$\Delta_q = \frac{2}{3} h_T = 2\frac{\sqrt{3}}{9}. \tag{60}$$

The associated nominal input set can be chosen as:

$$\bar{\mathbb{U}} \triangleq \{\bar{u} \in \mathbb{R} : |\bar{u}| \leq 2\Delta_q\}, \tag{61}$$

while terminal region can be characterized via:

$$\mathbb{X}_f \triangleq \left\{ x \in \mathbb{R}^n : |x - x^\star| \leq b = \frac{u_{\max} - |u^\star|}{|K|} = 1.3 \right\} \tag{62}$$

which provides that

$$|\eta_{\mathbb{U}}(\bar{u})| \leq \Delta_q = 2\frac{\sqrt{3}}{9} \tag{63}$$

for all $x \in \mathbb{X}_f$. Now, it is possible to verify that condition (27) in Theorem 1 is satisfied by:

$$\Delta_q^2 = 0.1481 < \left(\frac{a_1 - a_2\rho}{a_4}\right) b^2 = 0.3825. \tag{64}$$

Thus, one can anticipate that the system state, x, will be led by the predictive controller to the ultimately invariant set:

$$\mathcal{D}_\delta \triangleq \{x \in \mathbb{R}^n : |x - x^\star| \leq \delta = 0.8088\}. \tag{65}$$

Here, it is assumed that, for safety reasons, the converter will work in the following range:

$$\mathbb{X} = \{x \in \mathbb{R}^2 : x_1 \in [0 \;\; 7.5], x_2 \in [-2.5 \;\; 2.5]\}. \tag{66}$$

Using Algorithm 1, one obtains that $X_{MPC} = \mathbb{X}$.

The evolution of the 2-level inverter under horizon-one FCS-MPC, starting from $i_d = i_q = 0$, is depicted in Fig. 14. Here, one can see that the predictive controller leads the system state to the terminal region, $\mathbb{X}_f$, and then to the invariant bounded set $\mathcal{D}_\delta$. As expected for this kind of controller, the inverter voltage spectrum is spread. This can be observed in Fig. 15, yielding a distortion per phase of $\text{THD}_\text{v} = 1.3367\ \%$. Nevertheless, it can be noticed that system achieved a non-zero average steady-state error.

To improve this behaviour, based on the analysis carried out for the buck DC-DC converter, the value of R is reduced to

$$R = 0.0001 I_{2\times 2}. \tag{67}$$

This gives us the following cost function setting:

$$P \cong I_{2\times 2}, \quad K = \begin{bmatrix} -0.8249 & -0.0267 \\ 0.0267 & -0.8249 \end{bmatrix}. \tag{68}$$

The results of this new settings are presented in Figs. 16 and 17. In the latter, one can observed that the inverter voltage pattern is different to the one shown in Fig. 15. This is due to the fact that the matrix R directly affects the control input. For the case shown in Fig. 15, i.e., $R > Q$ the predictive controller gives more importance to minimize the input action, $u - u^\star$, than the state tracking error, $x - x^\star$. Thus, with this new settings, the harmonic pollution in the inverter voltage is higher than the one obtained when $R > Q$. More specifically, $\text{THD}_\text{v} = 2.2802\ \%$. Consequently, by reducing R, the steady-state average error was reduced as expected. However, similar to a Linear Quadratic Regulator, the controller dynamic is increased, resulting in a more aggressive controller [27]. This can be noticed in an increment of the switching frequency since the controller is trying to compensate higher frequency current errors. Therefore, there is a trade off between steady-state error and power switches losses.

VII. Conclusions

When controlling solid-state power converters in discrete-time, in general, voltages and currents will not converge to the desired steady-state values. This motivates the analysis of such converters from a practical stability viewpoint, i.e., by studying convergence of state variables to a bounded invariant set. The results presented here show how the cost function of FCS-MPC can be designed to obtain a desired performance while guaranteeing practical stability of the power converter. As documented via simulation and experimental results, this analysis can be used to characterize the controller performance, in terms of transient response and steady state error, by determining the decay rate of the tracking error and the size of the ultimately bounded set respectively.

Future work may focus on extending the results presented in this paper to more complex power converter topologies and also to develop novel high-performance controllers. Another interesting topic is to further investigate the effect of the input weighting matrix R on the switching frequency and spectrum. Additionally, based on [26], the extension of this work for larger horizon formulation can be also investigated.

References

[1] S. Kouro, M. Malinowski, K. Gopakumar, J. Pou, L. Franquelo, B. Wu, J. Rodríguez, M. A. Pérez, and J. Leon, "Recent Advances and Industrial Applications of Multilevel Converters," *IEEE Transactions on Industrial Electronics*, vol. 57, no. 8, pp. 2553–2580, 2010.

[2] T. Geyer, "Computationally Efficient Model Predictive Direct Torque Control," *IEEE Transactions on Power Electronics*, vol. 26, no. 10, pp. 2804–2816, 2011.

[3] P. Cortés, M. P. Kazmierkowski, R. M. Kennel, D. E. Quevedo, and J. Rodríguez, "Predictive Control in Power Electronics and Drives," *IEEE Transactions on Industrial Electronics*, vol. 55, no. 12, pp. 4312–4324, Dec. 2008.

[4] S. Kouro, P. Cortés, R. Vargas, U. Ammann, and J. Rodríguez, "Model Predictive Control—A Simple and Powerful Method to Control Power Converters," *IEEE Transactions on Industrial Electronics*, vol. 56, no. 6, pp. 1826–1838, Jun. 2009.

[5] J. Rodríguez, M. P. Kazmierkowski, J. Espinoza, P. Zanchetta, H. Abu-Rub, H. A. Young, and C. A. Rojas, "State of the Art of Finite Control Set Model Predictive Control in Power Electronics," *IEEE Transactions on Industrial Informatics*, vol. 9, no. 2, pp. 1003–1016, May 2013.

[6] T. Geyer, "A Comparison of Control and Modulation Schemes for Medium-Voltage Drives: Emerging Predictive Control Concepts Versus PWM-Based Schemes," *IEEE Transactions on Industry Applications*, vol. 47, no. 3, pp. 1380–1389, 2011.

[7] S. Vazquez, J. Leon, L. Franquelo, J. Rodríguez, H. A. Young, A. Marquez, and P. Zanchetta, "Model Predictive Control: A Review of Its Applications in Power Electronics," *IEEE Industrial Electronics Magazine*, vol. 8, no. 1, pp. 16–31, 2014.

[8] J. Rawlings and D. Mayne, *Model Predictive Control: Theory and Design*. Nob Hill Publishing, 2009.

[9] D. E. Quevedo, R. P. Aguilera, M. A. Pérez, P. Cortés, and R. Lizana, "Model Predictive Control of an AFE Rectifier With Dynamic References," *IEEE Transactions on Power Electronics*, vol. 27, no. 7, pp. 3128–3136, 2012.

[10] D. du Toit, H. d. T. Mouton, R. Kennel, and P. Stolze, "Predictive Control of Series Stacked Flying-Capacitor Active Rectifiers," *IEEE Transactions on Industrial Informatics*, vol. 9, no. 2, pp. 697–707, 2013.

[11] T. J. Vyncke, S. Thielemans, and J. A. Melkebeek, "Finite-Set Model-Based Predictive Control for Flying-Capacitor Converters: Cost Function Design and Efficient FPGA Implementation," *IEEE Transactions on Industrial Informatics*, vol. 9, no. 2, pp. 1113–1121, 2013.

[12] R. P. Aguilera, P. Lezana, and D. E. Quevedo, "Finite-Control-Set Model Predictive Control With Improved Steady-State Performance," *IEEE Transactions on Industrial Informatics*, vol. 9, no. 2, pp. 658–667, May 2013.

[13] V. Yaramasu, M. Rivera, M. Narimani, B. Wu, and J. Rodríguez, "Model Predictive Approach for a Simple and Effective Load Voltage Control of Four-Leg Inverter With an Output *LC* Filter," *IEEE Transactions on Industrial Electronics*, vol. 61, no. 10, pp. 5259–5270, 2014.

[14] M. Preindl and S. Bolognani, "Model Predictive Direct Torque Control With Finite Control Set for PMSM Drive Systems, Part 1: Maximum Torque Per Ampere Operation," *IEEE Transactions on Industrial Informatics*, vol. 9, no. 4, pp. 1912–1921, 2013.

[15] ——, "Model Predictive Direct Torque Control With Finite Control Set for PMSM Drive Systems, Part 2: Field Weakening Operation," *IEEE Transactions on Industrial Informatics*, vol. 9, no. 2, pp. 648–657, 2013.

[16] J. Scoltock, T. Geyer, and U. K. Madawala, "A Comparison of Model Predictive Control Schemes for MV Induction Motor Drives," *IEEE Transactions on Industrial Informatics*, vol. 9, no. 2, pp. 909–919, 2013.

[17] D. E. Quevedo, G. C. Goodwin, and J. A. De Doná, "Finite constraint set receding horizon quadratic control," *International Journal of Robust and Nonlinear Control*, vol. 14, no. 4, pp. 355–377, Jan. 2004.

[18] R. P. Aguilera and D. E. Quevedo, "On stability and performance of finite control set MPC for power converters," in *Workshop on Predictive Control of Electrical Drives and Power Electronics (PRECEDE)*, Oct. 2011, pp. 55–62.

[19] A. Bemporad, M. Morari, V. Dua, and E. N. Pistikopoulos, "The explicit linear quadratic regulator for constrained systems," *Automatica*, vol. 38, pp. 3–20, 2002.

[20] H. Khalil, *Nonlinear Systems (3rd Edition)*. Prentice Hall, 2001.

[21] P. Lezana, R. P. Aguilera, and D. E. Quevedo, "Model Predictive Control of an Asymmetric Flying Capacitor Converter," *IEEE Transactions on Industrial Electronics*, vol. 56, no. 6, pp. 1839–1846, 2009.

[22] D. E. Quevedo, R. P. Aguilera, and T. Geyer, "Predictive Control in Power Electronics and Drives: Basic Concepts, Theory, and Methods," in *Studies in Computational Intelligence*. Cham: Springer International Publishing, Jan. 2014, pp. 181–226.

[23] T. Geyer and D. E. Quevedo, "Multistep Finite Control Set Model Predictive Control for Power Electronics," *IEEE Transactions on Power Electronics*, vol. 29, no. 12, pp. 6836–6846, 2014.

[24] ——, "Performance of Multistep Finite Control Set Model Predictive Control for Power Electronics," *IEEE Transactions on Power Electronics*, no. 99, p. 1, 2014.

[25] K. J. Åström and B. Wittenmark, *Computer-Controlled Systems: Theory and Design*, 3rd ed. Prentice Hall, 1997.

[26] R. P. Aguilera and D. E. Quevedo, "Stability Analysis of Quadratic MPC with a Discrete Input Alphabet," *IEEE Transactions on Automatic Control*, vol. 58, no. 12, pp. 3190–3196, Dec. 2013.

[27] K. J. Åström and R. M. Murray, *Feedback Systems: An Introduction for Scientists and Engineers*. Princeton University Press, 2010.

[28] D. Limón, T. Álamo, D. Raimondo, D. de la Peña, J. Bravo, A. Ferramosca, and E. Camacho, "Input-to-state stability: a unifying framework for robust model predictive control," in *Nonlinear Model Predictive Control*, L. Magni, D. Raimondo, and F. Allgöwer, Eds. Springer Berlin / Heidelberg, 2009, pp. 1–26.

APPENDIX A
PROOF OF THEOREM 1

Firstly, the notion of *practical* stability is reviewed. The term "practical" is used to emphasize that only stability to a neighbourhood of the reference can be guaranteed.

Definition 1: (Practical-Lyapunov Function) A (not necessarily continuous) function $V : \mathbb{R}^n \to \mathbb{R}_{\geq 0}$ is said to be a *practical*-Lyapunov function (LF) in a region $\mathcal{A} \subseteq \mathbb{R}^n$ for the system (1) if there exist a compact set $\Omega \subseteq \mathcal{A}$, some positive constants a_1, a_2, a_3, d, σ, and $l \geq 1$ such that

$$V(x) \geq a_1|x|^l, \qquad \forall x \in \mathcal{A}, \quad (69)$$

$$V(x) \leq a_2|x|^l + d, \ \forall x \in \Omega, \quad (70)$$

$$\Delta V(x) = V(x(k+1)) - V(x) \leq -a_3|x|^l + \sigma, \quad (71)$$

for all $x \in \mathcal{A}$.

Theorem 2: (Converse theorem [28]) If system (1) admits a practical-LF in $\mathcal{A}$, then it is Practically Asymptotically Stable (PAS) in $\mathcal{A}$. ■

The above theorem tells one that, if one can find a practical-LF for the system to be controlled, then it is *practically asymptotically stable*. In other words, a practical-LF provides *sufficient conditions* for the existence of a controller $u(x) = \kappa(x)$ which ensures asymptotic (exponential) stability to a neighbourhood of the reference for the system (10). This stability concept is illustrated in Fig. 1.

Proof: (Theorem 1) To prove stability of the closed-loop (10), the following candidate LF is considered

$$V_f(x(k)) = (x(k) - x^\star)^T P (x(k) - x^\star). \quad (72)$$

Then, for this particular candidate LF the conditions presented in Definition 1 are verified.

Firstly, notice that conditions (69) and (70) are satisfied when $l = 2$, $a_1 = \lambda_{\min}(P)$, $a_2 = \lambda_{\max}(P)$, and $d = 0$, i.e.,

$$a_1|x - x^\star|^2 \leq V_f(x) \leq a_2|x - x^\star|^2. \quad (73)$$

Then, to analyze condition (71), one can obtain that (with $x(k) = x$ and $\tilde{x} = \tilde{x}(k) = x(k) - x^\star$)

$$\begin{aligned} \Delta V_f(x) &= V_f(x(k+1)) - V_f(x) \\ &\leq V_f(x(k+1)) - V_f(x) + |\tilde{u}^{\text{opt}}(x)|_R^2 \\ &= |A\tilde{x} + B\tilde{u}^{\text{opt}}(x)|_P^2 - |\tilde{x}|_P^2 + |\tilde{u}^{\text{opt}}(x)|_R^2 \\ &= \tilde{x}^T (A_K^T P A_K - P + K^T R K)\tilde{x} + |\eta_{\mathbb{V}}(x)|^2 \\ &\quad + 2\tilde{x}^T (A_K^T P B + K^T R) W^{-1/2} \eta_{\mathbb{V}}(x) \end{aligned} \quad (74)$$

where $\tilde{u}^{\text{opt}}(x)$ is as in (16), and W is as per (14). Since matrix P is chosen according to (18), it follows that

$$\begin{aligned} A_K^T P A_K - P + K^T R K &= -Q \\ A_K^T P B + K^T R = A^T P B + K^T (B^T P B + R) &= 0. \end{aligned} \quad (75)$$

Thus, it can be confirmed that

$$\Delta V_f(x) \leq -\tilde{x}^T Q \tilde{x} + |\eta_{\mathbb{V}}(x)|^2. \quad (76)$$

Notice that the quantization error $\eta_{\mathbb{V}}$ may differ from $\eta_{\mathbb{U}}$. However, for any $\bar{u} \in \mathbb{R}^m$, the quantization error can be bounded as

$$\begin{aligned} |\eta_{\mathbb{V}}(\bar{u})| &\leq |q_{\mathbb{V}}\left(W^{1/2}\bar{u}\right) - W^{1/2}\bar{u}| \\ &\leq |W^{1/2} q_{\mathbb{U}}(\bar{u}) - W^{1/2}\bar{u}| \\ &\leq |W|^{1/2} |q_{\mathbb{U}}(\bar{u}) - \bar{u}| \\ &\leq |W|^{1/2} \eta_{\mathbb{U}}(\bar{u}). \end{aligned} \quad (77)$$

The, the following relationship is obtained

$$\Delta V_f(x) \leq -a_3|x - x^\star|^2 + a_4|\eta_{\mathbb{U}}(x)|^2, \quad \forall x \in \mathbb{R}^n. \quad (78)$$

Considering the case where $x(k) = x \in \mathbb{X}_f$, from (24), it follows that $|\eta_{\mathbb{U}}(x)| \leq \Delta_q$, which allows one to obtain

$$\Delta V_f(x) \leq -a_3|x - x^\star|^2 + a_4\Delta_q^2, \quad \forall x \in \mathbb{X}_f \quad (79)$$

Therefore, property (71) holds with $a_3 = \lambda_{\min}(Q)$, $a_4 = |W|$, and $\sigma = a_4\Delta_q^2$ for all $x \in \mathbb{X}_f$.

Now, considering that $V_f(x) \leq a_2|x|^2$, see (73), it is possible to establish the following relationship

$$V_f(x(k+1)) \leq \rho V_f(x(k)) + a_4\Delta_q^2, \quad \forall x(k) \in \mathbb{X}_f, \quad (80)$$

which implies that

$$|\tilde{x}(k+1)|^2 \leq \frac{a_2}{a_1}\rho|\tilde{x}|^2 + \frac{a_4}{a_1}\Delta_q^2, \quad \forall x(k) \in \mathbb{X}_f. \tag{81}$$

Notice that $\rho \in [0, 1)$.

Suppose that $x(k) \in \mathbb{X}_f$, i.e., $|x(k)| \leq b$. and that the quantization error is bounded as in (27), from (81), it follows that

$$|\tilde{x}(k+1)|^2 \leq \frac{a_2}{a_1}\rho b^2 + \frac{a_4}{a_1}\frac{(a_1 - a_2\rho)}{a_4}b^2 = b^2, \tag{82}$$

thus $x(k+1) \in \mathbb{X}_f$, which implies that $\mathbb{X}_f$ is an invariant set for the closed-loop system (10).

Now, it is necessary to determine in which region the candidate-LF, $V_f(x)$, is monotonically decreasing, i.e., $\Delta V_f(x) < 0$. Notice that as the system state, x, moves away from the reference, the first term, $-a_3|x - x^\star|^2$ becomes more negative. However, the quantization error also increases making $a_4|\eta_{\mathbb{U}}(x)|^2$ larger. Thus, a region of attraction where the horizon-one FCS-MPC can stabilize the system is given by:

$$X_{MPC} \triangleq \mathbb{X}_f \cup \{x \in \mathbb{R}^n \backslash \mathbb{X}_f : g(x) < 0\}, \tag{83}$$

where $g(x) = \Delta V_f(x)$. This condition is introduced in Theorem 1, as (29) and is used in the Algorithm 1. Therefore, for any initial state $x(0) \in X_{MPC} \backslash \mathbb{X}_f$, there exists a finite instant $t > 0$, such that $x(k) \in \mathbb{X}_f$ for all $k \geq t$.

By iterating (80) for an initial condition $x(t)$, it follows that

$$V_f(x(k)) \leq \rho^k V_f(x(t)) + \left(\frac{1-\rho^k}{1-\rho}\right) a_4\Delta_q^2, \tag{84}$$

for all $x(t) \in \mathbb{X}_f$. Taking into account (73), it can be confirmed that

$$\tilde{x}(k) \leq \frac{a_2}{a_1}\rho^k\tilde{x}(t) + \left(\frac{1-\rho^k}{1-\rho}\right)\frac{a_4}{a_1}\Delta_q^2, \quad \forall x(k) \in \mathbb{X}_f. \tag{85}$$

Therefore, for all $x(t) \in \mathbb{X}_f$, it follows that

$$\limsup_{k\to\infty} |x(k) - x^\star| \leq \delta \tag{86}$$

as presented in (28). Consequently, $V_f(x)$ in (72) is a practical-LF in X_{MPC} for the closed-loop system (10) with $\mathcal{D}_\delta$ in (25) as an ultimately bounded set. ■

Ricardo P. Aguilera (S'02–M'11) received his B.Sc. degree in Electrical Engineering from the Universidad de Antofagasta, Chile, in 2003, his M.Sc. degree in Electronics Engineering from the Technical University Federico Santa Maria, Chile, in 2007, and his Ph.D. degree in Electrical Engineering from The University of Newcastle, Australia, in 2012.

From 2003 to 2004, he was a Research Assistant at the Technical University Federico Santa Maria, Chile. Then, from 2012 to 2013, he was a Research Academic at the School of Electrical Engineering and Computer Science at The University of Newcastle, Australia, where he was part of the Centre for Complex Dynamic Systems and Control. In January 2013, he joined the School of Electrical Engineering and Telecommunications at The University of New South Wales (UNSW), Sydney, Australia, where he currently holds a Senior Research Associate position at the Australian Energy Research Institute (AERI). His research interests are at the intersection of power electronics and modern control theory with main emphasis on model predictive control.

Daniel E. Quevedo (S'97–M'05–SM'14) received Ingeniero Civil Electrónico and Magister en Ingeniería Electrónica degrees from the Universidad Técnica Federico Santa María, Valparaíso, Chile in 2000. In 2005, he received the Ph.D. degree from The University of Newcastle, Australia, where he is currently an Associate Professor. He has been a visiting researcher at various institutions, including Uppsala University, KTH Stockholm, Kyoto University, Karlsruher Institut fr Technologie, University of Notre Dame, INRIA Grenoble, The Hong Kong University of Science and Technology, Aalborg University, and NTU Singapore.

Dr. Quevedo was supported by a full scholarship from the alumni association during his time at the Universidad Técnica Federico Santa María and received several university-wide prizes upon graduating. He received the IEEE Conference on Decision and Control Best Student Paper Award in 2003 and was also a finalist in 2002. In 2009 he was awarded a five-year Australian Research Fellowship. His research interests include several areas within automatic control, signal processing, and power electronics.